Applied Surface Science 392 (2017) 297–304

Contents lists available at ScienceDirect

Applied Surface Science

journal homepage: www.elsevier.com/locate/apsusc

# Low-crystallinity molybdenum sulfide nanosheets assembled on carbon nanotubes for long-life lithium storage: Unusual electrochemical behaviors and ascending capacities

Xiaodan Li [a], Gaoxiang Wu [a], Jiewei Chen [a], Meicheng Li [a,b,*], Wei Li [c], Tianyue Wang [a], Bing Jiang [a], Yue He [a], Liqiang Mai [d]

[a] State Key Laboratory of Alternate Electrical Power System with Renewable Energy Sources, North China ElectricPower University, Beijing, 102206, China
[b] Chongqing Materials Research Institute, Chongqing 400707, China
[c] International Iberian Nanotechnology Laboratory (INL), Braga 4715-330, Portugal
[d] State Key Laboratory of Advanced Technology for Materials Synthesis and Processing, Wuhan University of Technology, Wuhan 430070, China

ARTICLE INFO

*Article history:*
Received 24 July 2016
Received in revised form
10 September 2016
Accepted 12 September 2016
Available online 14 September 2016

*Keywords:*
Low-crystallinity molybdenum sulfide
Nanosheets
Long-life
Lithium-ion batteries

ABSTRACT

Low-crystallinity molybdenum sulfide (LCMS, Mo:S = 1:2.75) nanosheets synthesized by a facile and low temperature solvothermal method is now reported. The as-prepared LCMS anode material is composited of $MoS_2$ layers mixed with amorphous $MoS_3$, which leads to an unusual electrochemical process for lithium storage compared to typical $MoS_2$ anode. The existence of $MoS_3$ and Mo (VI) provide strong adsorption and binding sites for polar polysulphides, which compels abundant sulfur to turn into new-formed $MoS_3$ rather than diffuse into electrolyte. To fully utilize this novel electrochemical process, LCMS is decorated on carbon nanotubes, obtaining well-dispersed CNTs@LCMS. As electrode material for lithium storage, CNTs@LCMS exhibits a noticable ascending trend in capacity from 820 mA h $g^{-1}$ to 1350 mA h $g^{-1}$ at 100 mA $g^{-1}$ during 130 cycles. The persistent ascending capacity is ascribed to the increasing lithium storage caused by new-formed $MoS_3$, combined with the reduced volume change benifiting from well-dispersed CNTs@LCMS. Furthermore, the ascending performance is proved to be able to effectively extend the circulation life (up to 200%) for lithium-ion batteries by mathematical modeling and calculation. Accordingly, the CNTs@LCMS composite is a promising anode material for long-life lithium-ion batteries.



## 1. Introduction

Lithium-ion secondary batteries, with high specific energy and power densities, have dominated the power source field for portable electronic devices [1–5]. In order to meet the increasing huge power requirements of electric vehicles and the power storage for certain renewable energy sources, such as solar and wind energy, enormous efforts have been made to develop high-performance lithium-ion batteries (LIBs), especially the electrode materials [6–10]. In this context, many metal oxides or sulfides have been intensively explored as alternative anode materials for lithium storage due to their relatively high energy density, environmental friendliness and low-cost [3,6,8]. In particular, $MoS_2$ has been considered as an attractive LIBs anode material in view of its facile synthesis and the capability to allow easy lithium ions insertion/extraction, enabling its assembly with diverse substrates and delivering a high theoretical specific capacity of 670 mA h $g^{-1}$ [11]. Various $MoS_2$ nanostructures such as nanoplates [12], nanotubes [13] and nanoflowers [14] have been reported for lithium storage as LIB anodes which showed high capacities. However, large volume changes often occur in the $MoS_2$ anode during repeated charge and discharge process, which causes pulverization and aggregation, hence resulting in quick capacity fading upon cycling. Furthermore, the reaction process of $MoS_2$ generally involves insulating polysulfides ($Li_2S_x$, $1 < x < 8$) which could easily dissolve in liquid electrolyte, causing dissolution loss of electrode, deteriorated the conductivity of the electrolyte and the electrode, thus leading to capacity fading [15–17].

* Corresponding author at: State Key Laboratory of Alternate Electrical Power System with Renewable Energy Sources, North China Electric Power University, Beijing, 102206, China.
*E-mail addresses:* xiaodan_li@yeah.net (X. Li), wgxjimmy@126.com (G. Wu), kzscjw@126.com (J. Chen), mcli@ncepu.edu.cn (M. Li), wei.li@inl.int (W. Li), 1355796015@qq.com (T. Wang), BingJiang@ncepu.edu.cn (B. Jiang), 947667748@qq.com (Y. He), mlq518@whut.edu.cn (L. Mai).

http://dx.doi.org/10.1016/j.apsusc.2016.09.055
0169-4332/

Amorphization of active materials has been considered as an effective approach to improve the cycling stability and specific capacity. Firstly, the isotropic and open structure in amorphous materials can effectively tolerate the anisotropic expansion caused by the insertion of lithium ions and reducing stresses deriving from phase transition [18,19]. The comparatively slight volume changes were demonstrated in the amorphous silicon and tin oxide based anodes [20–22]. Secondly, amorphous materials possess a lower reactions change in Gibbs free energy ($\Delta G$) compared to its crystallinity counterpart, which contributes to the enhanced reversibility of conversion reaction for amorphous anode [23]. For example, the amorphous $Fe_2O_3$, $MnO_x$ and $MoO_2$ have been reported to exhibit higher capacity and better cyclability than crystallinity one [23–25]. In addition, amorphous $MoS_3$ present steadily reversible electrochemical performance for lithium storage and Mo (VI) with high affinity for sulfur-containing molecules can reduce the dissolution of polysulfides, benefiting the capacity and cyclability of electrode [19,26]. On the other hand, active materials were usually immobilized into/onto various matrices to suppress their capacity fade during cycling, such as carbon nanofiber, carbon nanotube (CNT), graphene [26–28].

In this work, we report the synthesis of a low-crystallinity molybdenum sulfide (LCMS, Mo:S = 1:2.75) by a facile and low temperature solvothermal approach. The LCMS is likely the mixture of layered $MoS_2$ and amorphous $MoS_3$, indicated by XPS, ICP and TEM characterization. The LCMS shows an unusual electrochemical behaviour in the lithium ion storage, distinct from those of previous studies of $MoS_2$-based materials [26,29,30] and $MoS_x$/CNTs [31]. When the LCMS was directly loaded on pristine CNTs to build a new composite anode (CNTs@LCMS) for LIBs, a phenomenon of ascending capacity upon cycling appears. Furthermore, a mathematical modelling and calculation demonstrates that the phenomenon of ascending capacity caused by this abnormal electrochemical process can effectively extend the circulation life of lithium-ion batteries.

## 2. Experimental section

### 2.1. Materials synthesis

#### 2.1.1. Chemicals

The carbon nanotubes (CNTs) were purchased from Nanocyl, Belgium. The $(NH_4)_2MoS_4$ powder and *N*, *N*-dimethylformamide (DMF) were purchased from Sigma-Aldrich, Australia. All chemicals were used as received without further purification.

#### 2.1.2. Preparation of the CNTs@LCMS composite

0.1 g of CNTs was dispersed into 30 mL of *N*, *N*-dimethylformamide (DMF) by ultrasonication for 20 min. Then, 0.22 g of $(NH_4)_2MoS_4$ powder was added in the solution. After stirring for 10 min, the homogeneous solution was transferred into a 35 mL Teflon-lined stainless steel autoclave and kept in an electric oven at 180 °C for 24 h. The autoclave was then left to cool down to room temperature naturally. The black precipitate was collected by centrifugation, thoroughly washed with deionized water and ethanol for several times and dried at 70 °C for 12 h in vacuum.

For comparison, the as-prepared CNTs@LCMS composite was further annealed at 800 °C in an atmosphere of 5% of $H_2$ balanced by Ar at a ramping rate of 5 °C $min^{-1}$ and maintained at this temperature for 2 h in order to convert amorphous $MoS_3$ into high-crystallinity $MoS_2$, resulting in the CNTs@$MoS_2$ composite.

#### 2.1.3. Preparation of LCMS clusters

LCMS clusters were prepared by the same method as mentioned above, in the absence of CNTs.

### 2.2. Characterization

The distribution, size and morphology of the as-prepared samples were characterized by the scanning electron microscopy (SEM) (FEI SIRION 200). Transmission electron microscopy (TEM), high-resolution TEM (HRTEM), high-angle annular dark-field scanning transmission electron microscopy (HAADF-STEM) and EDX mapping studies were carried out on a probe-corrected transmission electron microscope operating at 200 kV (FEI Tecnai F20). The chemical compositions and structures of the as-prepared samples were analysed by X-ray diffraction (XRD) (Bruker D8 Advance X-ray diffractometer, Cu-Kα radiation λ = 0.15406 nm) and X-ray photoelectron spectroscopy (XPS) (AXIS Ultra-DLD, Kratos Analytical, Manchester, UK, using monochromated Al Kα radiation). The exact Mo:S molar ratio in the LCMS clusters was also measured by the inductively coupled plasma optical emission spectroscopy (ICP-OES, Agilent 730). The LCMS clusters were digested into the solution using a mixed acid method. Then the resulting solution was diluted appropriately and measured for the Mo and S elements (molar ratio, Mo: S = 1:2.75) by the ICP-OES.

### 2.3. Electrochemical measurements

The working electrodes were fabricated by coating a slurry containing 80 wt% of active materials (CNTs@LCMS, CNTs@$MoS_2$ or LCMS clusters), 10 wt% of acetylene black (Super-P), and 10 wt% of polyvinylidene fluoride (PVDF) dissolved in *N*-methyl-2-pyrrolidinone onto a copper foil and dried at 100 °C in vacuum for 12 h before pressing. Standard CR2032-type coin cells were assembled in an Ar-filled glovebox (KIYON, Korea) by using the as-prepared anode, Li metal foil (0.4 mm thick) as the counter electrode, and a separator (Solupor 7P03A). The electrolyte was composed of 1 M $LiPF_6$ dissolved in a mixture of ethylene carbonate (EC) and dimethyl carbonate (DMC) (V/V = 1:1). The cells were aged for 12 h before the measurements. Galvanostatic discharge–charge (GDC) experiments were performed at different current densities in the voltage range of 0.01–3.00 V with a multichannel battery tester (Maccor, Inc, USA). Cyclic voltammetry (CV) measurements were conducted by the electrochemical workstation (Solartron Potentiostat and Impedance Analyser, UK). Electrochemical impedance spectra (EIS) were measured using the same electrochemical workstation by applying an AC voltage of 10 mV amplitude over the frequency range from 100 kHz to 0.1 Hz.

## 3. Results and discussion

The bare low-crystallinity molybdenum sulfide (LCMS) powder and CNTs@LCMS composite were synthesized by solvothermal decomposition of $(NH_4)_2MoS_4$ at 180 °C. The bare LCMS powders are composed of clusters with an average size of 100 nm, which are actually agglomerated by many LCMS nanosheets, as shown in Fig. 1a. When adding CNTs, the LCMS nanosheets grow on the surface of CNTs to form a cable-like nanostructure with favorable dispersion (Fig. 1b). At this mass ratio $(NH_4)_2MoS_4$ to CNTs (2.2:1), LCMS nanosheets are uniformly anchored onto the originally smooth CNTs (Fig. S1) without any aggregation in the resulting CNTs@LCMS composite. Fig. 1c shows the TEM image and corresponding fast Fourier transform (FFT) pattern of a typical LCMS nanosheet in LCMS clusters, demonstrating the clear layered structure of $MoS_2$ and some amorphous component ($MoS_3$). In the CNTs@LCMS composite, LCMS nanosheets are anchored onto the surface of CNTs, as confirmed by TEM image and corresponding FFT

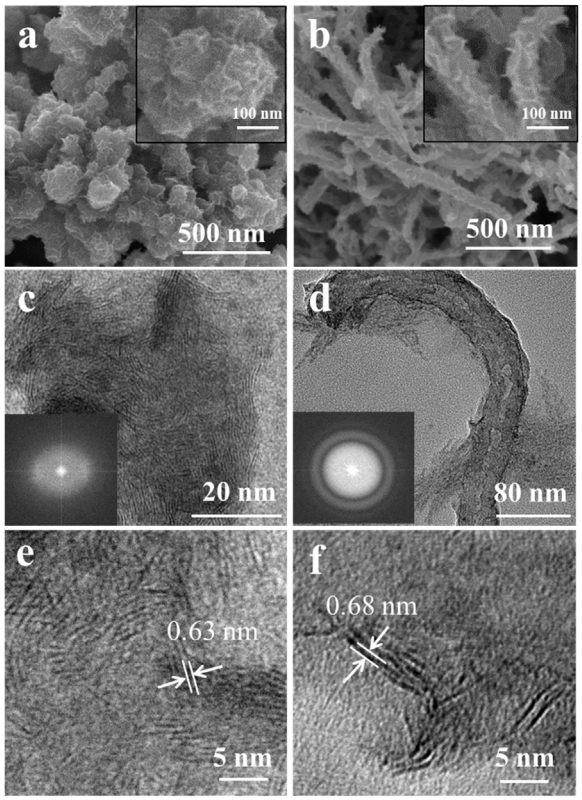


**Fig. 1.** Structural characterization: SEM images of LCMS clusters (a) and CNTs@LCMS composite (b). TEM images of LCMS clusters (c) and CNTs@LCMS composite (d). HRTEM images of LCMS clusters (e) and CNTs@LCMS composite (f).

pattern in Fig. 1d. Both LCMS clusters and CNTs@LCMS give the low crystallinity nature. Meanwhile, the XRD patterns (Fig. S2) of LCMS and CNTs@LCMS present wide diffraction peaks rather than sharp diffraction peaks of the $MoS_2$ [6], which demonstrate their low crystallinity. The HRTEM image of a LCMS cluster (Fig. 1e) displays that the typical interlayer spacing of $MoS_2$ layers in LCMS clusters is approximately 0.63 nm, corresponding to the (002) plane. The lattice fringe of (002) plane was also observed in the CNTs@LCMS composite (Fig. 1f), despite enlarged spacing of 0.68 nm, possibly due to the undulated surface of $MoS_2$ nanosheets and expansion of coaxial structure [26,32]. Accordingly, LCMS nanosheet composited of $MoS_2$ layers mixed with amorphous $MoS_3$ and its composite (CNTs@LCMS) are successfully obtained.

The chemical compositions of CNTs@LCMS were examined by energy dispersive X-ray spectroscopy (EDX). The EDX spectrum exhibits the presence of C, S and Mo in the CNTs@LCMS composite. Fig. 2 shows the HAADF-STEM image of the CNTs@LCMS composite and corresponding EDX elemental maps of C, S and Mo, confirming the homogeneous distribution of Mo and S over the entire carbon nanotube. In addition, the inductively coupled plasma (ICP) analysis demonstrates that the S:Mo molar ratio of LCMS clusters is estimated to be 2.75, confirming the existence of sulfur-rich phase ($MoS_3$).

The chemical states of Mo, S, and C on the surface of LCMS clusters and CNTs@LCMS were further investigated by X-ray photoelectron spectroscopy (XPS). The high-resolution XPS spectrum (Fig. S3) shows that the obvious C1s peak of CNTs@LCMS is at 284.6 eV, assigned to a $sp^2$ hybridized carbon atom of CNTs, while the C 1s peak of LCMS clusters is quite weak, arising from the inevitable carbon contamination [33]. The high-resolution Mo 3d XPS spectra of LCMS clusters and CNTs@LCMS were deconvoluted, as shown in Fig. 3. The peaks at ~229 eV (3 $d_{5/2}$) and ~232 eV (3 $d_{3/2}$) can be assigned to the existence of Mo (IV) in $MoS_2$, consistent with literature. More importantly, a pair of peaks at ~230 eV and ~233 eV is present, which is normally attributed to Mo (VI) in amorphous $MoS_3$ [26,31]. A small peak at ~236 eV implies slight oxidation of LCMS on the surface formed during the process of preparation and exposure to air. As for the S 2p spectrum, it can be interpreted into two doublets for apical $S^{2-}$ or bridging disulfide $S_2^{2-}$ ligands, which are similar to those of amorphous $MoS_3$ [34,35]. In addition, the thermal decomposition of $(NH_4)_2MoS_4$ refers to the reduction of $S^{2-}$ ligands of the $MoS_4^{2-}$ anion and the oxidation of molybdenum metal from $Mo^{4+}$ to $Mo^{6+}$ [36]. Thus, it is proposed that amorphous $MoS_3$ was formed in both LCMS cluster and CNTs@LCMS, due to the uncompleted redox caused by low temperature.

The as-prepared samples were then assembled into Li half-cells to investigate the electrochemical performance. Fig. 4a, b present the galvanostatic discharge–charge (GDC) voltage profiles of the LCMS clusters and CNTs@LCMS in the potential window of 0.001–3 V at a current density of 100 mA $g^{-1}$, respectively. Upon

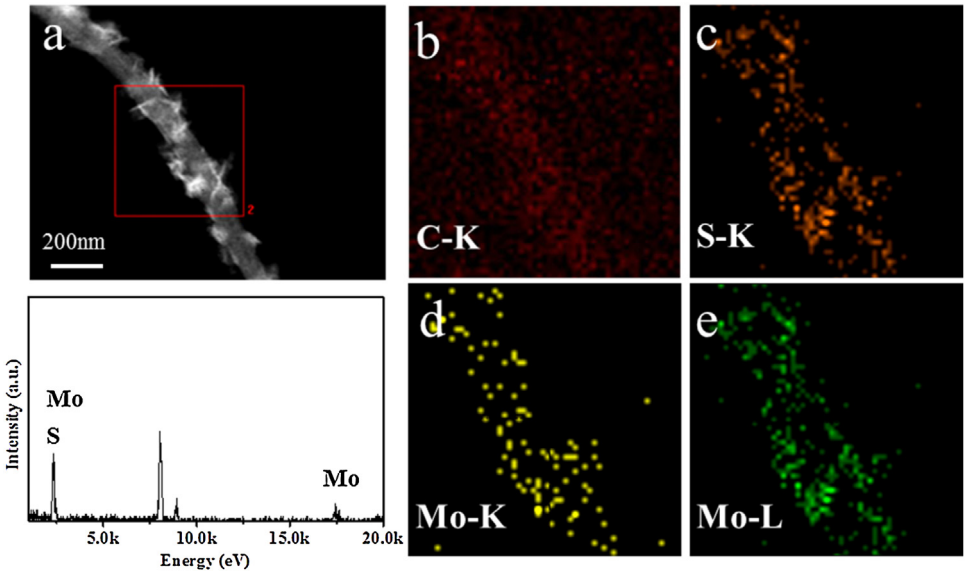


**Fig. 2.** (a) HAADF-STEM images of CNTs@LCMS; (b–e) EDX elemental mappings of CNTs@LCMS for C, S, and Mo, respectively.

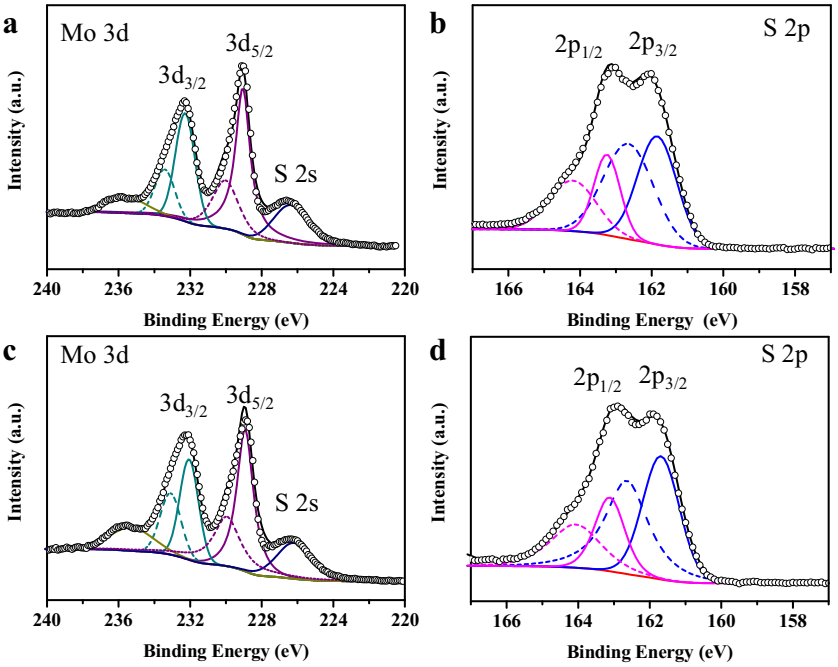


**Fig. 3.** XPS spectra of LCMS clusters (a, b) and CNTs@LCMS (c, d) for Mo and S element.

initial discharge, a slope profile occurs at 1.6–1.1 V, involving a multiple lithiation process of the LCMS. An apparent voltage plateau at ~0.6 V is diminished in the subsequent was usually assigned to the conversion process of $Li_xMoS_2$ to Mo nanocrystals embedded in a $Li_2S$ matrix [19,37,38]. The charge profile shows plateaus at approximately 1.85 V and 2.3 V, which are due to the formation of $Mo^{6+}$ and the oxidation of $Li_2S$ [19,26]. The initial discharge and charge specific capacities of LCMS clusters are 1236 and 964 mA h $g^{-1}$, respectively, leading to a Coulombic efficiency (CE) of 78%. When the LCMS are immobilized onto CNTs, the CNTs@LCMS composite exhibits discharge and charge specific capacities of 1180 and 820 mA h $g^{-1}$, with a Coulombic efficiency of 70% in the first cycle. Compositing with carbon nanotubes would partly sacrifice the high theoretical capacity of LCMS and enhance the formation of SEI film, resulting in lower initial capacity and Coulombic efficiency (CE). However, it is interesting that the specific capacity of CNTs@LCMS increases continually from 820 mA h $g^{-1}$ to 1350 mA h $g^{-1}$ during 100 cycles, while LCMS exhibits an increasing capacity just in the first several cycles and capacity fading thereafter. Meanwhile, the specific capacity of CNTs@$MoS_2$ decreases normally upon cycling (Fig. 4c). Apparently, the unique structure and component of CNTs@LCMS leads to an obvious synergistic effect. Large volume change occurs in the aggregated LCMS clusters, which will cause electrical disconnection to current collectors. In this case, LCMS clusters could not remain continuous increase in capacity during long time cycling even in the similar electrochemical process with CNTs@LCMS. Thus, the CNTs matrix with high electric conductivity not only relief the volume change of LCMS, but synergistically enhance the novel electrochemical process of LCMS, leading to an ascending capacity upon cycling.

Even at 1 A $g^{-1}$ (Fig. 4d), the specific capacity of CNTs@LCMS demonstrates the ascending trend to 720 mA h $g^{-1}$ in the first 210 cycles and retains at ~600 mA h $g^{-1}$ after 400 cycles. Moreover, upon gradually elevating the current density, CNTs@LCMS still delivers a high specific capacity of 530 mA h $g^{-1}$ even at 2 A $g^{-1}$, while the $MoS_2$ clusters and CNTs@$MoS_2$ can only deliver decreasing capacity of 50 mA h $g^{-1}$ and 440 mA h $g^{-1}$ at the 1 A $g^{-1}$, respectively (Fig. 4e). Upon decreasing the current density back to 0.1 A $g^{-1}$, the capacities of the CNTs@LCMS tend to surpass the initial capacity every time, indicating good recovery and ascending trend in capacity.

To reveal the electrochemistry essence of this ascending trend in capacity, cyclic voltammetry (CV) of the LCMS clusters and CNTs@LCMS were collected at a slow scan rate of 0.05 mV $s^{-1}$ in a potential window of 0.01–3.00 V vs. $Li^+$/Li, as shown in Fig. 5. During the initial discharge process, two cathodic peaks present the stepwise Li intercalation into LCMS followed by the conversion reaction of $MoS_2$ to Mo and $Li_2S$ (Fig. 5a). In the first anodic process, three anodic peaks appear at ~1.5 V, ~1.85 V and ~2.3 V, respectively. The small anodic peak at 1.5 V is due to the oxidations from Mo to $Mo^{4+}$ or Mo ions with a higher valence (eg. $Mo^{6+}$) [19,26]. And the pronounced peaks at ~1.85 V and ~2.3 V are associated with the electrochemical behavior of Mo and sulfur element deriving from amorphous $MoS_3$ [17]. The CV performance of CNTs@LCMS (Fig. 5b) also exhibits similar electrochemical reaction to LCMS clusters but extra sloped profiles at <0.3 V ascribed to the reversible lithiation/delithiation of CNTs [17,26,27].

In the subsequent CVs, the two pairs of peaks related to $MoS_3$ are still well-defined, indicating a reversible electrochemical process of amorphous $MoS_3$ for lithium storage. And a single anodic peak at ~1.5 V becomes waning, indicating the continuous consumption of unoxidized Mo to high-valence Mo ions. It is notable that the CV results of LCMS-based anodes present no cathodic peak at ~1.85 V corresponding to the reaction of Li and $S_8$ (Fig. 5), while this peak usually dominates the subsequent electrochemistry of typical $MoS_2$ anode [26,30,31]. It is clear that the amorphous $MoS_3$ around layered $MoS_2$ affect the electrochemical performance of LCMS for lithium storage. It is reported that $Mo^{6+}$ has ability to bind surrounding polysulfides due to its higher affinity for sulfur-containing molecules [32]. In this case, the oxidized sulfur element tends to mergers into new-formed $MoS_3$ rather than exists in form of polysulfur, resulting in the missing reaction peak of Li and $S_8$.

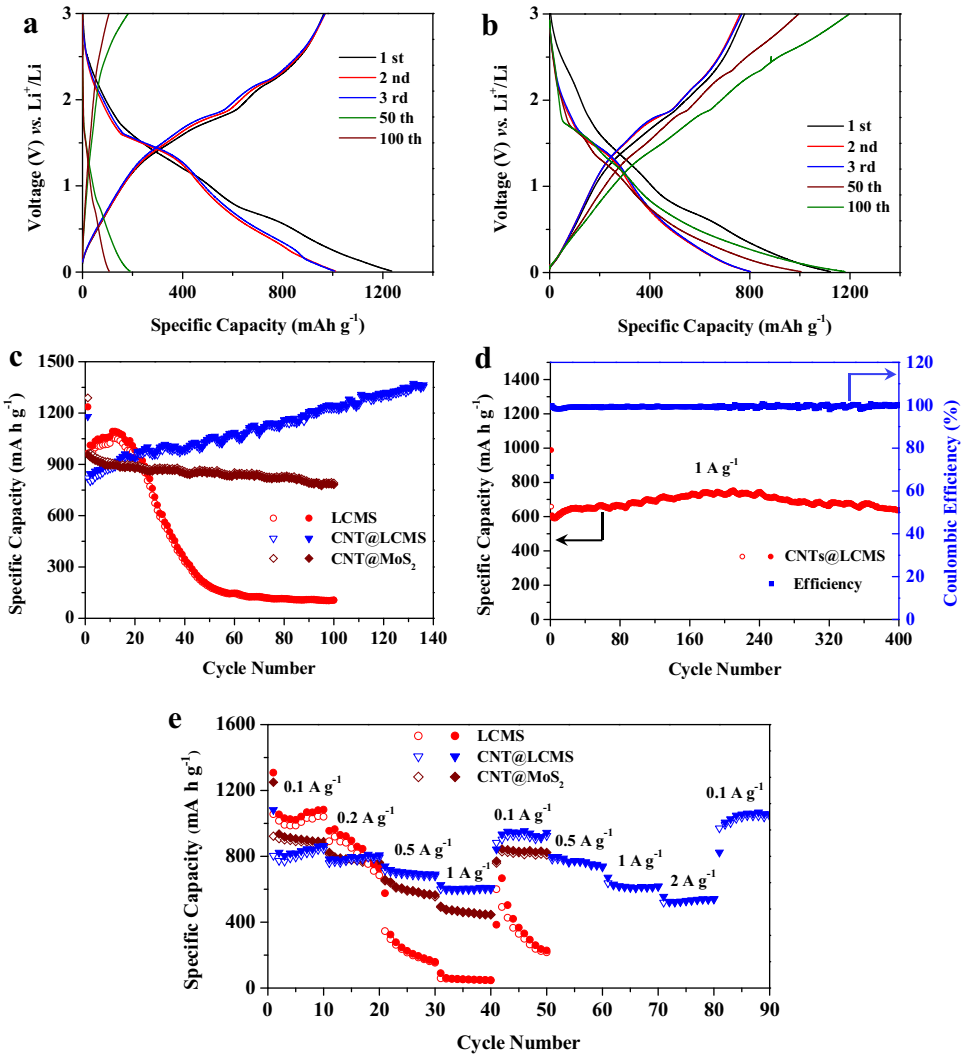


**Fig. 4.** Galvanostatic discharge-charge voltage profiles of LCMS clusters (a) and CNTs@LCMS (b) at a current density of 100 mA $g^{-1}$; (c) comparative cycling performance of LCMS clusters, CNTs@LCMS and CNT@$MoS_2$ at a current density of 100 mA $g^{-1}$; (d) long-life cycling performance of CNTs@LCMS at 1 A $g^{-1}$; and (e) rate performance of LCMS clusters, CNTs@LCMS and CNT@$MoS_2$ at different current densities.

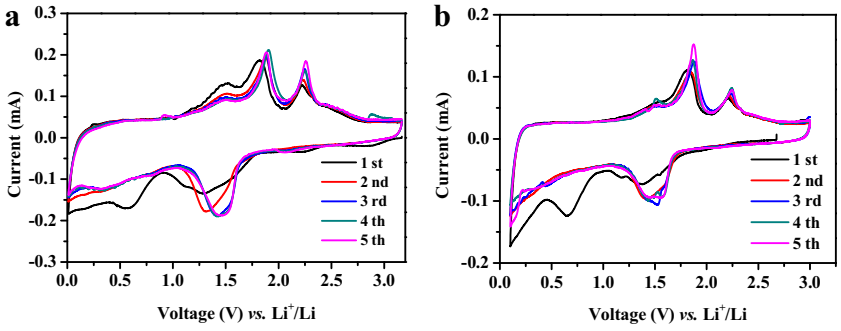


**Fig. 5.** Representative CV curve of LCMS clusters (a) and CNTs@LCMS (b) for the first five cycles at a scan rate of 0.05 mV $s^{-1}$.

Meanwhile, the new-formed $MoS_3$ enhance electrochemical utilization of Mo and sulfur, resulting in gradually increased anodic peak at ~1.85 V and ~2.3 V.

The electrochemical reactions of $MoS_2$ and $MoS_3$ could be described as follows:

$$Li^+ + MoS_2 \rightarrow Mo + Li_2S \quad \text{(I)}$$

$$Li^+ + MoS_3 \leftrightarrow Li_xMoS_3 \leftrightarrow Mo + Li_2S \quad \text{(II)}$$

According to Reaction (I), the lithiation of $MoS_2$ involves in the generation of $Li_2S$ (Lithium-sulfur reaction) and depends on the degree of reaction, thus its theoretical capacity is 667–1675 mA h $g^{-1}$ [11]. The practical capacity of $MoS_2$/C was reported up to be 1300 mA h $g^{-1}$ [11]. In Reaction (II), the $MoS_3$ is sulfur-rich material which leads to more and deeper lithium-sulfur reaction, thus the theoretical capacity should be much closer to 1675 mA h $g^{-1}$. On the other hand, the S:Mo molar ratio of 2.75

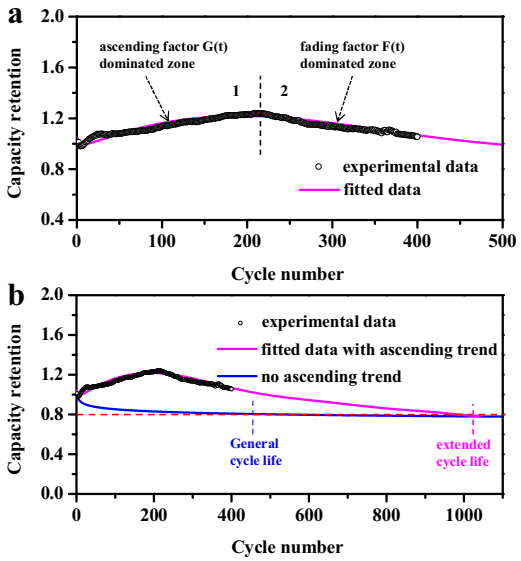


**Fig. 6.** Modeling and calculation: (a) Modeling analysis based on experimental data in Fig. 4d; (b) Prediction of the circulation lives for lithium-ion batteries with and without ascending trend.

confirmed by ICP analysis could predict the content of $MoS_3$ in LCMS is about 75%, resulting in a high capacity of 1350 mA h $g^{-1}$.

For the hollow or porous materials which are difficult to be infiltrated by electrolyte or Li-ion, the capacities sometimes show a short-time ascending trend in the early charge/discharge process, usually called active process. And several kinds of active materials would present increasing capacities after tens of cycles at high current density. In our case, the capacity of CNTs@LCMS anode demonstrates a regular ascending trend during long-time cycles. And the ascending trend in capacity during cycling occurs in duplicable tests, as shown in Fig. S4. Especially the capacities at different current density still keep increasing and tend to surpass the initial capacity every time decreasing the current density back to smaller one.

Therefore, the evident ascending trend at various current densities upon cycling is attributed to the unique electrochemistry of CNTs@LCMS, distinguished from normal active process or other circumstances. Upon discharging, amorphous $MoS_3$ demonstrated a reversible lithiation/delithiatin process, while the $MoS_2$ existed in LCMS was intercalated by Li and transformed into Mo nanoparticles and $Li_2S$, as shown in Scheme 1. Generally, these $Li_2S$ generated during the initial discharge process just can be partly oxidized to $S_8$ due to the diffusion loss of soluble polysulfides into electrolyte upon charging (Scheme 1a), which usually deteriorate the capacity and cyclability of $MoS_2$, such as CNT@$MoS_2$ in Fig. 4c, d [11]. While in LCMS system (Scheme 1b), $Li_xMoS_3$ and $Mo^{6+}$ own high affinity for sulfur-containing molecules, which tend to adsorb or bind surrounding polysulfides, accelerating redox reactions of polysulphides and $Mo^{6+}$ for new-formed $MoS_3$, thus leads to low diffusion loss of soluble polysulfides [11,26,39]. On the whole, with the merging of electrochemically unstable S decomposed from $MoS_2$ into new-formed $MoS_3$ upon charging, LCMS exhibits stabilized and enhanced electrochemical utilization of sulfur compared to typical $MoS_2$. In addition, CNTs with high electronic conductivity act both as a Li storage matrix and as a conductive backbone for well-dispersed LCMS, resulting in improved kinetics for electron and lithium ion transport, enhanced oxidation to $Mo^{6+}$ and a minimized strain of volume changes. The structure and morphology of CNTs@LCMS after cycling test were characterized by SEM (Fig. S5, ESI†), which is in accordance with the above analysis. The unique electrochemical process for lithium storage and well-dispersed

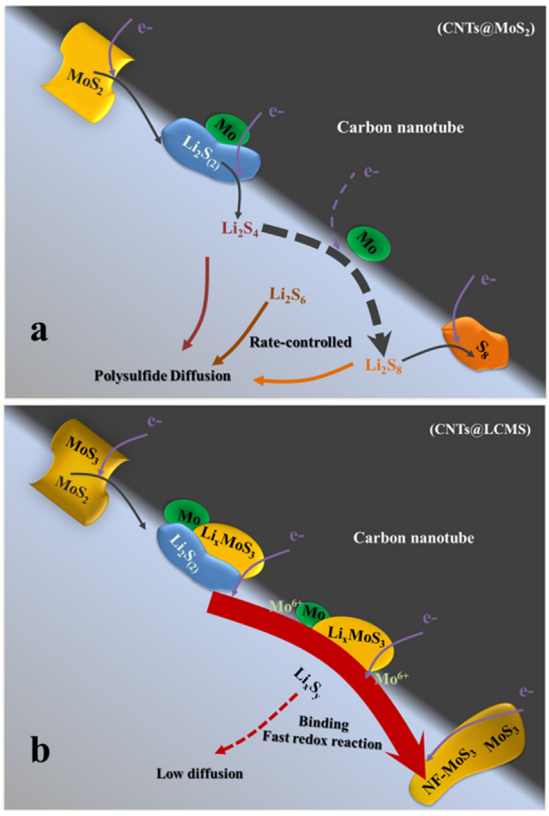


**Scheme 1.** Schematic illustration of lithiation/delithiation processes for typical CNT@$MoS_2$ (a) and CNTs@LCMS (b) anodes, in which NF-$MoS_3$ means new-formed $MoS_3$.

LCMS on CNTs with high electric conductivity synergistically leads to the long-lasting ascending capacity of CNTs@LCMS.

Electrochemical-impedance-spectroscopy (EIS) results show that compared to LCMS clusters, CNTs@LCMS exhibit significantly reduced charge-transfer resistances ($R_{ct}$) before and after cycling (Fig. S6). Therefore, the kinetic performance of CNTs@LCMS composite is improved upon cycling, which is consistent with the above analysis.

Moreover, due to the ascending trend in capacity, the charge capacity of the CNTs@LCMS was even the same as the initial charge capacity after 400 cycles at current density of 1 A $g^{-1}$ (Fig. 4d). Therefore, it could be deduced that the ascending performance involving the unique electrochemical process can extend the circulation life of lithium-ion batteries. To confirm this deduction, modeling calculation combined with experimental data was employed for the quantitative analysis. Considering that the formation and continuous thickening of the SEI film on the surface of the anode materials, Eq. (1) is widely used in the capacity retention modeling for the lithium ion batteries: [40,41]

$$F(t) = B\exp\left(\frac{-E_a}{RT}\right)t^z \quad (1)$$

Where F(t) is the percentage of battery capacity retention; $E_a$ is the activation energy in J $mol^{-1}$; R is the gas constant; T is the absolute temperature in K; t is the cycling time; z is the power law factor; and B is the pre-exponential factor. While in our work, the new-formed $MoS_3$ which causes ascending capacity should be considered as another factor. This factor obeys a monotone increasing function which has the limit, as described in Eq. (2):

$$G(t) = A\exp(ht) + C \quad (2)$$

In which A, h and C are fitted constants. Thus, based on the correction of the Eqs. (1) and (2) combined with fitting process of the

experimental data (Fig. 6a), a new capacity retention model can be presented as follows:

$$Q_{ret}(t) = B\exp(\frac{-E_a}{RT})t^z + k(t)\{Aexp(ht) + C\} \quad (3)$$

Finally the new model is employed to predict the circulation life for our lithium ion batteries, shown as Fig. 6b. End of life is usually defined as when the battery reaches 80% of its initial capacity [4]. According to the mathematical modeling, the circulation lives of LIBs with and without ascending process are predicted to be roughly 1000 and 500 cycles at current density of $1\,A\,g^{-1}$, respectively. These results demonstrate that the phenomenon of ascending capacity caused by this novel electrochemical process can effectively extend the circulation life of lithium-ion batteries.

## 4. Conclusions

In summary, low-crystallinity Molybdenum sulfide (LCMS, Mo:S=1:2.75) have been successfully developed by a facile and cost-effective low-temperature solvothermal method. Compared to typical $MoS_2$, LCMS demonstrated a novel electrochemical process for lithium storage, which is dominated by reversible lithiation/delithiation of $MoS_3$, accompanying a persistent oxidation of Mo and merger of sulfur to produce new-formed $MoS_3$. When the LCMS was dispersedly loaded on pristine CNTs, it exhibited an evident ascending trend in capacity from $820\,mA\,h\,g^{-1}$ to $1350\,mA\,h\,g^{-1}$ at $100\,mA\,g^{-1}$ during 130 cycles. Even at the current density of $1\,A\,g^{-1}$, the CNTs@LCMS anode exhibits an ascending capacity to $720\,mA\,h\,g^{-1}$ in the first 210 cycles. Combining with modelling calculation and experimental data, the ascending performance of CNTs@LCMS is proved to effectively extend the battery circulation life from 500 to 1000 cycles at $1\,A\,g^{-1}$, indicating that CNTs@LCMS composite is a promising anode material for long-life lithium-ion batteries.

## Acknowledgements

This work is supported partially by National High-tech R&D Program of China (863 Program, No.2015AA034601), National Natural Science Foundation of China (Grant nos. 91333122, 51402106, 51372082, 51172069, 61204064 and 51202067), Ph.D. Programs Foundation of Ministry of Education of China (Grant nos. 20120036120006, 20130036110012), Par-Eu Scholars Program, and the Fundamental Research Funds for the Central Universities.

## Appendix A. Supplementary data

Supplementary data associated with this article can be found, in the online version, at http://dx.doi.org/10.1016/j.apsusc.2016.09.055.

## References

[1] J.M. Tarascon, M. Armand, Issues and challenges facing rechargeable lithium batteries, Nature 414 (2001) 359–367.
[2] A.S. Arico, P. Bruce, B. Scrosati, J.M. Tarascon, W. van Schalkwijk, Nanostructured materials for advanced energy conversion and storage devices, Nat. Mater. 4 (2005) 366–377.
[3] X. Li, Y. Feng, M. Li, W. Li, H. Wei, D. Song, Smart hybrids of Zn2GeO4 nanoparticles and ultrathin g-C3N4 layers: synergistic lithium storage and excellent electrochemical performance, Adv. Funct. Mater. 25 (2015) 6858–6866.
[4] M. Armand, J.M. Tarascon, Building better batteries, Nature 451 (2008) 652–657.
[5] B. Kang, G. Ceder, Battery materials for ultrafast charging and discharging, Nature 458 (2009) 190–193.
[6] X. Li, W. Li, M. Li, P. Cui, D. Chen, T. Gengenbach, L. Chu, H. Liu, G. Song, Glucose-assisted synthesis of the hierarchical TiO2 nanowire@MoS2 nanosheet nanocomposite and its synergistic lithium storage performance, J. Mater. Chem. A 3 (2015) 2762–2769.
[7] D. Larcher, S. Beattie, M. Morcrette, K. Edstrom, J.-C. Jumas, J.-M. Tarascon, Recent findings and prospects in the field of pure metals as negative electrodes for Li-ion batteries, J. Mater. Chem. 17 (2007) 3759–3772.
[8] Y. Feng, X. Li, Z. Shao, H. Wang, Morphology-dependent performance of Zn2GeO4 as a high-performance anode material for rechargeable lithium ion batteries, J. Mater. Chem. A 3 (2015) 15274–15279.
[9] L. Chu, M. Li, X. Li, Y. Wang, Z. Wan, S. Dou, D. Song, Y. Li, B. Jiang, High performance NiO microsphere anode assembled from porous nanosheets for lithium-ion batteries, RSC Adv. 5 (2015) 49765–49770.
[10] P. Cui, B. Xie, X. Li, M. Li, Y. Li, Y. Wang, Z. Liu, X. Liu, J. Huang, D. Song, J.M. Mbengue, Anatase/TiO2-B hybrid microspheres constructed from ultrathin nanosheets: facile synthesis and application for fast lithium ion storage, CrystEngComm 17 (2015) 7930–7937.
[11] T. Stephenson, Z. Li, B. Olsen, D. Mitlin, Lithium ion battery applications of molybdenum disulfide (MoS2) nanocomposites, Energ. Environ. Sci. 7 (2014) 209–231.
[12] H. Hwang, H. Kim, J. Cho, MoS2 nanoplates consisting of disordered graphene-like layers for high rate lithium battery anode materials, Nano Lett. 11 (2011) 4826–4830.
[13] R. Dominko, D. Arcon, A. Mrzel, A. Zorko, P. Cevc, P. Venturini, M. Gaberscek, M. Ramskar, D. Mihailovic, Dichalcogenide nanotube electrodes for Li-ion batteries, ChemInform 34 (2003) 1531–1534.
[14] H. Li, W. Li, L. Ma, W. Chen, J. Wang, Electrochemical lithiation/delithiation performances of 3D flowerlike MoS2 powders prepared by ionic liquid assisted hydrothermal route, J. Alloy Compd. 471 (2009) 442–447.
[15] Y. Kim, J.B. Goodenough, Lithium insertion into transition-metal monosulfides: tuning the position of the metal 4s band, J. Phys. Chem. C 112 (2008) 15060–15064.
[16] X. Wang, Q. Xiang, B. Liu, L. Wang, T. Luo, D. Chen, G. Shen, TiO2 modified FeS nanostructures with enhanced electrochemical performance for lithium-ion batteries, Sci. Rep. 3 (2013) 10454–10461.
[17] L. Ji, M. Rao, H. Zheng, L. Zhang, Y. Li, W. Duan, J. Guo, E.J. Cairns, Y. Zhang, Graphene oxide as a sulfur immobilizer in high performance lithium/sulfur cells, J. Am. Chem. Soc. 133 (2011) 18522–18525.
[18] Q. Fan, P.J. Chupas, M.S. Whittingham, Characterization of amorphous and crystalline tin–cobalt anodes, Electrochem. Solid State 10 (2007).
[19] T. Matsuyama, A. Hayashi, T. Ozaki, S. Mori, M. Tatsumisago, Electrochemical properties of all-solid-state lithium batteries with amorphous MoS3 electrodes prepared by mechanical milling, J. Mater. Chem. A 3 (2015) 14142–14147.
[20] E. Hüger, L. Dörrer, J. Rahn, T. Panzner, J. Stahn, G. Lilienkamp, H. Schmidt, Lithium transport through nanosized amorphous silicon layers, Nano Lett. 13 (2013) 1237–1244.
[21] X. Li, X. Meng, J. Liu, D. Geng, Y. Zhang, M.N. Banis, Y. Li, J. Yang, R. Li, X. Sun, M. Cai, M.W. Verbrugge, Tin oxide with controlled morphology and crystallinity by atomic layer deposition onto graphene nanosheets for enhanced lithium storage, Adv. Funct. Mater. 22 (2012) 1647–1654.
[22] H. Ghassemi, M. Au, N. Chen, P.A. Heiden, R.S. Yassar, In situ electrochemical lithiation/delithiation observation of individual amorphous Si nanorods, ACS Nano 5 (2011) 7805–7811.
[23] Y. Jiang, D. Zhang, Y. Li, T. Yuan, N. Bahlawane, C. Liang, W. Sun, Y. Lu, M. Yan, Amorphous Fe2O3 as a high-capacity, high-rate and long-life anode material for lithium ion batteries, Nano Energy 4 (2014) 23–30.
[24] J. Guo, Q. Liu, C. Wang, M.R. Zachariah, Interdispersed amorphous MnOx–carbon nanocomposites with superior electrochemical performance as lithium-storage material, Adv. Funct. Mater. 22 (2012) 803–811.
[25] J.H. Ku, J.H. Ryu, S.H. Kim, O.H. Han, S.M. Oh, Reversible lithium storage with high mobility at structural defects in amorphous molybdenum dioxide electrode, Adv. Funct. Mater. 22 (2012) 3658–3664.
[26] F. Zhou, S. Xin, H.-W. Liang, L.-T. Song, S.-H. Yu, Carbon nanofibers decorated with molybdenum disulfide nanosheets: synergistic lithium storage and enhanced electrochemical performance, Angew. Chem. Int. Ed. 53 (2014) 11552–11556.
[27] D. Shujiang, C. Jun Song, X.W.D. Lou, Glucose-assisted growth of MoS2 nanosheets on CNT backbone for improved lithium storage properties, Chemistry (Weinheim an der Bergstrasse, Germany) 17 (2011) 13142–13145.
[28] K. Chang, W. Chen, L-Cysteine-assisted synthesis of layered MoS2/graphene composites with excellent electrochemical performances for lithium ion batteries, ACS Nano 5 (2011) 4720–4728.
[29] X. Zhou, Z. Wang, W. Chen, L. Ma, D. Chen, J.Y. Lee, Facile synthesis and electrochemical properties of two dimensional layered MoS2/graphene composite for reversible lithium storage, J. Power Sources 251 (2014) 264–268.
[30] P. Seung-Keun, Y. Seung-Ho, W. Seunghee, Q. Bo, L. Dong-Chan, K.M. Kun, S. Yung-Eun, P. Yuanzhe, A simple L-cysteine-assisted method for the growth of MoS2 nanosheets on carbon nanotubes for high-performance lithium ion batteries, Dalton Trans. 42 (2012) 2399–2405.
[31] Y. Shi, Y. Wang, J.I. Wong, A.Y.S. Tan, C.-L. Hsu, L.-J. Li, Y.-C. Lu, H.Y. Yang, Self-assembly of hierarchical MoSx/CNT nanocomposites (2<x<3): towards high performance anode materials for lithium ion batteries, Sci. Rep. 3 (2013) 2169.
[32] Z. Hu, L. Wang, K. Zhang, J. Wang, F. Cheng, Z. Tao, J. Chen, MoS2 nanoflowers with expanded interlayers as high-performance anodes for sodium-Ion batteries, Angew. Chem. Int. Ed. 53 (2014) 12794–12798.

[33] F. Dong, S. Guo, H. Wang, X. Li, Z. Wu, Enhancement of the visible light photocatalytic activity of C-Doped $TiO_2$ nanomaterials prepared by a green synthetic approach, J. Phys. Chem. C 115 (2011) 13285–13292.
[34] D. Merki, S. Fierro, H. Vrubel, X. Hu, Amorphous molybdenum sulfide films as catalysts for electrochemical hydrogen production in water, Chem. Sci. 2 (2011) 1262–1267.
[35] Y.-H. Chang, C.-T. Lin, T.-Y. Chen, C.-L. Hsu, Y.-H. Lee, W. Zhang, K.-H. Wei, L.-J. Li, Highly efficient electrocatalytic hydrogen production by MoSx grown on graphene-protected 3D Ni foams, Adv. Mater. 25 (2013) 756–760.
[36] T. Weber, J.C. Muijsers, J.W. Niemantsverdriet, Structure of amorphous MoS3, J. Phys. Chem. 99 (1995) 9194–9200.
[37] J. Zhou, J. Qin, X. Zhang, C. Shi, E. Liu, J. Li, N. Zhao, C. He, 2D space-confined synthesis of few-layer MoS2 anchored on carbon nanosheet for lithium-Ion battery anode, ACS Nano 9 (2015) 3837–3848.
[38] L. Yang, S. Wang, J. Mao, J. Deng, Q. Gao, Y. Tang, O.G. Schmidt, Hierarchical MoS2/polyaniline nanowires with excellent electrochemical performance for lithium-ion batteries, Adv. Mater. 25 (2013) 1180–1184.
[39] L. Wang, Z. Xu, W. Wang, X. Bai, Atomic mechanism of dynamic electrochemical lithiation processes of MoS2 nanosheets, J. Am. Chem. Soc. 136 (2014) 6693–6697.
[40] P. Ramadass, B. Haran, R. White, B.N. Popov, Mathematical modeling of the capacity fade of Li-ion cells, J. Power Sources 123 (2003) 230–240.
[41] L. Lu, X. Han, J. Li, J. Hua, M. Ouyang, A review on the key issues for lithium-ion battery management in electric vehicles, J. Power Sources 226 (2013) 272–288.